A Quasi-Vortex-Lattice Method in Thin Wing Theory

C. Edward Lan*
The University of Kansas, Lawrence, Kan.

A quasi-continuous method is developed for solving the thin wing problems. For the purpose of satisfying the wing boundary conditions, the spanwise vortex distribution is assumed to be stepwise constant while the chordwise vortex integral is reduced to a finite sum through a modified trapezoidal rule and the theory of Chebychev polynomials. Wing edge and Cauchy singularities are accounted for. The total aerodynamic characteristics are obtained by an appropriate quadrature integration. The two-dimensional results for airfoils without flap deflection reproduce the exact solutions in lift and pitching moment coefficients, the leading edge suction, and the pressure difference at a finite number of points. For a flapped airfoil, the present results are more accurate than those given by the vortex lattice method. The three dimensional results also show an improvement over the results of the vortex lattice method. Extension to nonplanar applications is discussed.

Nomenclature

A = aspect ratio
$\mathbf{a}$ = $(x_1 - x)\mathbf{i} + (y_1 - y)\mathbf{j} + (z_1 - z)\mathbf{k}$
$\mathbf{a}'$ = $(x_1 - x)\mathbf{i} + \beta(y_1 - y)\mathbf{j} + \beta(z_1 - z)\mathbf{k}$
$a.c.$ = aerodynamic center measured from the leading edge of the mean chord defined by $(2/S_w)\ {}_0\int^{b/2} c^2 dy$ and referred to the mean chord
a_{ij} = downwash influence coefficient
b = span
$\mathbf{b}$ = $(x_2 - x)\mathbf{i} + (y_2 - y)\mathbf{j} + (z_2 - z)\mathbf{k}$
$\mathbf{b}'$ = $(x_2 - x)\mathbf{i} + \beta(y_2 - y)\mathbf{j} + \beta(z_2 - z)\mathbf{k}$
c = local chord
$\bar{c}$ = average chord, S_w/b
C = square-root singularity parameter in $\gamma(x)$ defined in Eq. (15)
c_l = sectional lift coefficient
c_m = sectional pitching moment coefficient
C_{Di} = far-field induced drag coefficient
C_{Dii} = near-field induced drag coefficient
$C_{L\alpha}$ = lift curve slope, per radian
C_m = total pitching moment coefficient based on S_w and the average chord S_w/b, about the y-axis
C_s = leading-edge suction parameter
c_t = sectional leading-edge thrust coefficient
C_T = total leading-edge thrust coefficient
$\mathbf{l}$ = $(x_2 - x_1)\mathbf{i} + (y_2 - y_1)\mathbf{j} + (z_2 - z_1)\mathbf{k}$
$\mathbf{l}'$ = $(x_2 - x_1)\mathbf{i} + \beta(y_2 - y_1)\mathbf{j} + \beta(z_2 - z_1)\mathbf{k}$
$M-1$ = number of interpolation stations over the whole span
M_1-1 = number of spanwise vortex strips in region 1
M_2-1 = number of spanwise vortex strips in region 2
M_∞ = freestream Mach number
m = number of collocation stations
N, N_c = number of chordwise vortices
N_s = total number of spanwise vortex strips
$\mathbf{q}$ = induced velocity vector
$\mathbf{R}$ = $x\mathbf{i} + y\mathbf{j} + z\mathbf{k}$
R_β^2 = $(x - x')^2 + \beta^2(y - y')^2 + \beta^2(z - z')^2$
S = leading edge suction
S_w = wing area
x,y,z = wing rectangular coordinate system with x in the streamwise direction and y to the right
w = downwash, referred to the freestream velocity
z_c = camber
α = angle of attack
β = $(1 - M_\infty^2)^{1/2}$
γ = nondimensional vortex density referred to local chord and freestream velocity
Λ = leading-edge sweep angle

Subscripts
1 = the first endpoint of a vortex element
2 = the second endpoint of a vortex element
l = leading edge
t = trailing edge

Received June 19, 1973; revision received April 25, 1974. This research is part of a project supported by NASA Grant 17-002-107.
Index category: Airplane and Component Aerodynamics.
*Associate Professor of Aerospace Engineering. Member AIAA.

I. Introduction

IN the conventional vortex lattice method (VLM), the lifting surface (or thin airfoil) is divided into a number of small lifting elements (boxes). The continuous vortex distribution representing the wing in a uniform flow is replaced with a discrete one, where a vortex element is placed at each elemental quarter chord of the small boxes. The flow tangency condition is satisfied at each elemental three-quarter chord. Reasonable results by this method have been reported in the past.[1,2] For more references on the previous developments of this method, see Ref. 1. However, some characteristics of the conventional VLM are worth noting: 1) The method used to compute the induced drag implies that the leading edge thrust is distributed over the chord, instead of being concentrated at the leading edge, as has been criticized by Hancock.[3] 2) The predicted pressure distribution is accurate only away from the leading edge. Near the leading edge, the predicted pressure level is always too low, not only in the three-dimensional case,[2] but also in the two-dimensional theory.[4] 3) The convergence of solutions (C_L, C_m, and C_{Dii}/C_L^2) is slow with respect to the number of elements used, in particular for low aspect-ratio swept wings[1] and wings with flap deflection.[2] (After the completion of this research, Hough's paper appeared.[5] It seems that his method of using the ¼ lattice width inset at the wing tips improves the solution for a flat wing.) Some of the above difficulties may exist because the wing edge square-root singularities and the logarithmic singularity (in case of flap deflection) of the vortex distribution and the Cauchy singularity in the downwash integral have been completely ignored in the development of the VLM. The purpose of the present investigation is to improve the VLM through theoretical consideration so that the abovementioned singularities are accounted for in the method, yet retaining the simplicity of the VLM.

II. Two-Dimensional Theory

A) Conventional VLM

In the thin airfoil theory, the downwash on the airfoil is related to the vortex distribution through the following equation[6]:

Table 1 Comparison of thin airfoil vortex distribution

x	γ by VLM (10 elements)	Exact γ
0.025	11.070787	12.489996
0.125	5.244057	5.291503
0.225	3.701687	3.711843
0.325	2.879090	2.882307
0.425	2.325419	2.326320
0.525	1.902616	1.902380
0.625	1.550279	1.549193
0.725	1.233896	1.231764
0.825	0.925422	0.921132
0.925	0.582672	0.569495

$$w(x) = \frac{1}{2\pi} \int_0^1 \frac{\gamma(x')dx'}{x - x'} \tag{1}$$

where the coordinates are referred to the chord length. According to the conventional VLM, Eq. (1) is discretized to be[4]

$$2\pi w_i = \sum_j a_{ij}\gamma_j \tag{2}$$

where a_{ij} is given by

$$a_{ij} = \Delta x/(x_i - x_j) = 1/(1/2 + i - j) \tag{3}$$

In Eq. (2), $\gamma_j\Delta x$ represents the discrete vortex strength at the quarter-chord point of the jth element and γ_j is the vortex density at the same location in accordance with the traditional formulation.[1,2,4] Note that the difference in the surface pressure coefficients ΔC_p equals 2γ in the thin wing theory. The exact solution of Eq. (1) for $w(x) = 1$ can be shown to be

$$\gamma(x) = 2(1 - x)^{1/2}x^{-1/2} \tag{4}$$

The exact lift and moment coefficients are 2π and $-\pi/2$, respectively. Let $C_s = \lim_{x\to 0} u(x)\,(x)^{1/2}$. Then the suction force can be computed by[6]

$$S = \pi\rho C_s^2 \tag{5}$$

For a flat plate, $C_s = 1$.

To check the accuracy of the VLM, take $i = j = 1$ in Eq. (3). It follows that $a_{ij} = 2$ and hence, $\gamma(x) = \pi$ from Eq. (2) at $x = \frac{1}{4}$. But from the exact solution, Eq. (4), $\gamma(\frac{1}{4}) = 2(3)^{1/2}$, so that the VLM solution is too low. On the other hand, c_l is exact. In fact, it has been shown by James[4] that c_l and c_m obtained by VLM are always exact for any number of elements greater than 2. At least two elements are needed to compute c_m. To further examine the accuracy of the predicted $\gamma(x)$ for different number of elements, a few computer runs were made for 2–10 elements. Table 1 shows the results for 10 elements. It is seen that the primary error in the predicted $\gamma(x)$ occurs near the leading edge. The present computer results agree with James' analysis[4] that the first predicted γ-value is always 11.4% too low for large N.

Examination of Eqs. (1) and (2) reveals that the Cauchy singularity and the square-root singularities at the leading and trailing edges contained in $\gamma(x)$ have been completely ignored in the VLM. The conventional VLM was formulated from the standpoint of computing the over-all aerodynamic characteristics, instead of the local properties. Therefore, if the VLM is to be improved, the abovementioned singularities must be properly accounted for. This is being done in the following.

B) Present Analysis

Transforming the x-coordinate to the Θ-coordinate through the following relation

$$x = (1 - \cos\theta)/2 \tag{6}$$

Eq. (1) can be written as

$$w(\theta) = -\frac{1}{2\pi} \int_0^\pi \frac{\gamma(\theta')\sin\theta' d\theta'}{\cos\theta - \cos\theta'} \tag{7}$$

Let

$$g(\theta) = \gamma(\theta)\sin\theta \tag{8}$$

Then, to eliminate the Cauchy singularity in the integrand, Eq. (7) is rewritten as

$$\begin{aligned} w(\theta) = &-\frac{1}{2\pi} \int_0^\pi \frac{g(\theta') - g(\theta)}{\cos\theta - \cos\theta'} d\theta' \\ &- \frac{g(\theta)}{2\pi} \int_0^\pi \frac{d\theta'}{\cos\theta - \cos\theta'} \\ = &-\frac{1}{2\pi} \int_0^\pi \frac{g(\theta') - g(\theta)}{\cos\theta - \cos\theta'} d\theta' \end{aligned} \tag{9}$$

Now, $g(\Theta)$ does not contain the square-root singularities, because they have been eliminated by the factor $\sin\Theta$. Since the integrand in Eq. (9) is finite everywhere, the integral can be reduced to a finite sum through the midpoint trapezoidal rule.[7] It follows that

$$\begin{aligned} &\int_0^\pi \frac{g(\theta') - g(\theta)}{\cos\theta - \cos\theta'} d\theta' \\ &\quad \cong \Delta\theta' \sum_{k=1}^{N} \frac{g((2k-1)\Delta\theta'/2) - g(\theta)}{\cos\theta - \cos((2k-1)\Delta\theta'/2)} \\ &\quad = \frac{\pi}{N} \sum_{k=1}^{N} \left[\frac{g((2k-1)\pi/2N)}{\cos\theta - \cos((2k-1)\pi/2N)} \right. \\ &\qquad \left. - \frac{g(\theta)}{\cos\theta - \cos((2k-1)\pi/2N)} \right] \end{aligned} \tag{10}$$

where the last step is allowable if $\Theta \neq \Theta'$. In applications, it is convenient to eliminate the last term in Eq. (10). This can be done by choosing a particular set of control points, i.e., Θ-values in such a way that

$$\sum_{k=1}^{N} 1/(\cos\theta - \cos((2k-1)\pi/2N)) = 0 \tag{11a}$$

For this purpose, the theory of Chebychev polynomials will be used.

Let $\lambda_1\ \lambda_2, \ldots, \lambda_N$ be the zeros of $T_N(\lambda)$, the Chebychev polynomial of the first kind. Then for some constant K,

$$T_N(\lambda) = K(\lambda - \lambda_1)(\lambda - \lambda_2)\cdots(\lambda - \lambda_N)$$

and by logarithmic differentiation,

$$\sum_{k=1}^{N} 1/(\lambda - \lambda_k) = T_N'(\lambda)/T_N(\lambda) \tag{11b}$$

Now, if $\lambda = \cos\Theta$, it is known that $T_N(\cos\Theta) = \cos N\Theta$. The zeros of T_N are therefore $N\Theta_k = (2k-1)\pi/2$, or

$$\lambda_k = \cos\theta_k = \cos((2k-1)\pi/2N), k = 1, 2, \cdots, N \tag{12}$$

In order that Eq. (11a) be satisfied, Eq. (11b) shows that

$$T_N'(\lambda) = \frac{d}{d\theta}(\cos N\theta)\frac{d\theta}{d\lambda} = N\frac{\sin N\theta}{\sin\theta} \tag{13}$$

must vanish. This is true if $N\Theta_i = i\pi$, or

$$\lambda_i = \cos\theta_i = \cos(i\pi/N), i = 1, 2, \cdots, N-1 \tag{14}$$

For $i = N$, $\Theta_i = \pi$. From Eq. (13) it can be shown that $T_N'(\lambda_i) \to -N^2\cos N\pi$ and therefore $T_N'(\lambda_i)/T_N(\lambda_i) \to$

$-N^2$. This is the case where $\Theta = \pi$ in Eq. (6), or $x = 1$. But at $\Theta = \pi$, $g(\Theta) = \gamma(\Theta)\sin\Theta = 0$. Hence, the control points can be extended to $i = N$, i.e., the trailing edge without losing the validity of Eq. (11a). On the other hand, if $i = 0$, i.e., at the leading edge, it can be shown from Eq. (13) that $T_{N'}/T_N \to N^2$. Since the unknown function $\gamma(\Theta)$ is known to possess a square-root singularity at $\Theta = 0$, it follows that

$$\lim_{\theta\to 0} g(\theta) = \lim_{\theta\to 0} \gamma(\theta)\sin\theta = \lim_{x\to 0} C(1-x)^{1/2}x^{-1/2}\cdot 2x^{1/2}(1-x)^{1/2} = 2C \quad (15)$$

Hence, if the control points are chosen at $N + 1$ points, i.e., $i = 0, 1, \ldots N$, in Eq. (14), $(N + 1)$ unknowns, $\gamma_1, \gamma_2, \ldots, \gamma_N$, C can be computed. Note that the parameter C in Eq. (15) is related to the leading-edge suction parameter C_S. Since $u(x) = \gamma(x)/2$, it follows that

$$C_S = \lim_{x\to 0} u(x)x^{1/2} = \lim_{x\to 0} \gamma(x)x^{1/2}/2 = C/2 \quad (16)$$

If the singularity in γ is weaker than the square root singularity, then $C = 0$. It follows that the above-described procedures not only predict γ-values, but also the leading-edge suction directly.

Using the concept just described, Eq. (9) can now be reduced to

$$w(x_i) \cong \frac{1}{2N}\sum_{k=1}^{N} \frac{\gamma_k x_k^{1/2}(1-x_k)^{1/2}}{x_i - x_k} + \begin{cases} NC, & i = 0 \\ 0, & i \neq 0 \end{cases} \quad (17)$$

where

$$x_k = [1 - \cos((2k-1)\pi/2N)]/2, \; k = 1, 2, \cdots, N$$
$$x_i = [1 - \cos(i\pi/N)]/2, \quad i = 0, 1, \cdots, N \quad (18)$$

Eq. (17) can be written in a matrix form for the solution of γ as follows:

$$w_i = \sum_i a_{ik}\gamma_k \quad (19)$$

where

$$a_{ik} = \frac{1}{2N}\frac{x_k^{1/2}(1-x_k)^{1/2}}{x_i - x_k} \quad (19a)$$

Once γ_k''s are obtained, C can be computed as

$$C = \frac{w(\theta_0)}{N} + \frac{1}{2N^2}\sum_{k=1}^{N}\gamma_k\left(\frac{1-x_k}{x_k}\right)^{1/2} \quad (20)$$

The lift coefficient is given by

$$c_l = 2\int_0^1 \gamma(x)dx = \int_0^\pi \gamma(\theta)\sin\theta d\theta \cong \frac{\pi}{N}\sum_{k=1}^{N}\gamma_k\sin\theta_k \quad (21)$$

where Θ_k is given in Eq. (18). Similarly, the pitching moment coefficient about the leading edge can be shown to be

$$c_m = -2\int_0^1 \gamma(x)x dx = -\frac{1}{2}\int_0^\pi \gamma(\theta)(1-\cos\theta)\sin\theta d\theta \cong -\frac{\pi}{2N}\sum_{k=1}^{N}\gamma_k(1-\cos\theta_k)\sin\theta_k \quad (22)$$

To show the remarkable accuracy of the above formulation, take $N = 1$. Then $x_l = 1$, $x_k = \frac{1}{2}$ and $a_{ik} = \frac{1}{2}$. It follows that for $w = 1$, $\gamma_1 = 2$ at $x_k = \frac{1}{2}$. This result is exact, as can be seen from Eq. (4) by putting $x = \frac{1}{2}$. The lift coefficient is $c_l = 2\pi$, and the leading edge suction parameter C can be shown to be 2. Both are exact. c_m can not be correctly predicted when $N = 1$.

For $N = 2$, the matrix (a_{ik}) in Eq. (19) is

$$(a_{ik}) = \begin{pmatrix} 1/4 & -1/4 \\ 1/(4\cdot 2^{1/2}+4) & 1/(4\cdot 2^{1/2}-4) \end{pmatrix}$$

The solution for γ_k can be easily obtained to be $\gamma_1 = 2[1 + (2)^{1/2}]$ and $\gamma_2 = 2[(2)^{1/2} - 1]$. It follows from Eq. (20) that the suction parameter C is

$$C = 1/2 + [2(1 + 2^{1/2})^2 + 2(2^{1/2} - 1)^2]/8 = 2$$

The lift and pitching moment coefficients are

$$c_l = \pi[2^{1/2}(1 + 2^{1/2}) + 2^{1/2}(2^{1/2} - 1)]/2 = 2\pi$$

$$c_m = -\pi[2^{1/2}(1 + 2^{1/2})(1 - 2^{1/2}/2) + 2^{1/2}(2^{1/2} - 1)(1 + 2^{1/2}/2)]/4 = -\pi/2$$

It can be easily checked that the results for γ_k, C, c_l, and c_m are all exact.

For $N > 2$, computer runs were made for N up to 10. Again, all aerodynamic characteristics of interest are reproduced exactly.

To check whether the present method will work with the same accuracy for cases with camber, consider the case of parabolic camber. For $\gamma(x) = 2(x(1-x))^{1/2}$, it can be shown that

$$w(x) = \frac{1}{2\pi}\int_0^1 \frac{2(x'(1-x'))^{1/2}}{x - x'}dx' = x - 1/2.$$

c_l and c_m are

$$c_l = 2\int_0^1 \gamma(x)dx = \pi/2$$

$$c_m = -2\int_0^1 \gamma(x)x dx = -\pi/4.$$

Of course, the suction parameter C is zero for this case. Computer runs with $N = 5$ and 10 again reproduced the above results exactly.

The idea discussed above can be easily extended to a flapped airfoil. Let x_f be the nondimensional distance of flap hinge from the leading edge. Equation (1) will be written as sum of two integrals with the associated boundary conditions as follows:

$$w(x) = \frac{1}{2\pi}\int_0^{x_f}\frac{\gamma(x')dx'}{x - x'} + \frac{1}{2\pi}\int_{x_f}^1 \frac{\gamma(x')dx'}{x - x'} \quad (23a)$$
$$w(x) = 0, \quad 0 < x < x_f$$
$$w(x) = \delta, \quad x_f < x < 1$$

Let $x' = (x_f/2)(1 - \cos\Theta')$ in the first integral and $x' = x_f + (1 - x_f)(1 - \cos\Theta')/2$ in the second integral. Equation (23a) can therefore be transformed into the following expression:

$$w(x) = \frac{x_f}{4\pi}\int_0^\pi \frac{\gamma(\theta')\sin\theta' d\theta'}{x - x'(\theta')} + \frac{1 - x_f}{4\pi}\int_0^\pi \frac{\gamma(\theta')\sin\theta' d\theta'}{x - x'(\theta')} \quad (23b)$$

Again, the square-root singularities have been eliminated by the factor $\sin\Theta'$. In addition to the square-root singularities, $\gamma(\Theta')$ is known to behave like $\ln|\sin\Theta'|$ near the flap hinge. However, as $\Theta' \to \pi$ in the first integral and $\Theta' \to 0$ in the second integral, $\gamma(\Theta')\sin\Theta'$ behaves like $\sin\Theta\ln|\sin\Theta'|$ which is finite at the flap hinge. Therefore, the logarithmic singularity has been weakened in the

Table 2 Comparison of predicted vortex distributions for an airfoil with 30% flap chord and 30° flap deflection

A) Present method

x	γ by present method (8 elements)	Exact γ
0.01713	2.97703	2.98483
0.14427	1.12161	1.12482
0.35000	0.87234	0.87560
0.55572	0.95930	0.96778
0.68287	1.35336	1.56612
0.72010	1.36942	1.47857
0.85000	0.66955	0.66969
0.97990	0.20371	0.20357

B) VLM

x	γ by VLM (8 elements)	Exact γ
0.035	1.77634	2.11262
0.175	0.98106	1.04648
0.315	0.83379	0.88793
0.455	0.82308	0.88311
0.595	0.94419	1.03934
0.725	1.65671	1.40116
0.825	0.81856	0.76081
0.925	0.44945	0.42070

transformation. Each integral in Eq. (23b) will be Cauchy-singular only if the control point x is in that particular range of integration. When it is not Cauchy-singular, the integral can be directly approximated by a finite sum through the midpoint trapezoidal rule as described above. On the other hand, if it is Cauchy-singular, the singularity can be removed and the integral again approximated by a finite sum by the same method. The only difference lies in evaluating $\gamma(\Theta)\sin\Theta$ as $\Theta \to 0$. In the present case, it can be shown that

$$\lim_{\theta\to 0}\gamma(\theta)\sin\theta = \lim_{x\to 0} C(1-x)^{1/2}x^{-1/2}(2/x_f)(x(x_f-x))^{1/2} = 2C(x_f)^{-1/2} \tag{24}$$

Therefore, Eq. (23b) can be approximated by

$$w(x_i) \cong \frac{x_f}{4N_1}\sum_{k=1}^{N_1}\frac{\gamma(\theta_k)\sin\theta_k}{x_i - x_k} + \frac{1-x_f}{4N_2}\sum_{j=1}^{N_2}\frac{\gamma(\theta_j)\sin\theta_j}{x_i - x_j} + \begin{cases} N_1 C(x_f)^{-1/2}, & i = 0 \\ 0, & i \neq 0 \end{cases} \tag{25}$$

where N_1 and N_2 are the numbers of elements used for the first and the second integrals in Eq. (23b), respectively, and

$$x_k = (x_f/2)(1-\cos\theta_k), \theta_k = (2k-1)\pi/2N_1, k = 1, \cdots, N_1 \tag{26}$$

$$x_j = x_f + (1-x_f)(1-\cos\theta_j)/2, \theta_j = (2j-1)\pi/2N_2, j = 1, \cdots, N_2$$

In the range $[0, x_f]$, the control points are chosen so that

$$x_i = (x_f/2)(1-\cos\theta_i), \theta_i = i\pi/N_1, i = 0, 1, \cdots, N_1 \tag{27a}$$

while in the range $[x_f, 1]$, the control points are

$$x_i = x_f + (1-x_f)(1-\cos\theta_i)/2, \theta_i = i\pi/N_2, i = 1, 2, \cdots, N_2 \tag{27b}$$

Note that in Eq. (27a), $x_i = x_f$ for $i = N_1$. At this control point (i.e., at the flap hinge), $w(x_i)$ is discontinuous. In the present method, the average value is used. This is motivated by the results in the Fourier series analysis of discontinuous functions. Both c_l and c_m are obtained in a similar way as in Eqs. (21) and (22), except that each integral is approximated by two finite sums corresponding to two integration intervals as discussed above.

In order to accurately compare the relative efficiency and accuracy of the present method with the VLM, tabulated results are preferred. The exact solution of Eq. (23a) can be shown to be[6]

$$\gamma(x) = 2\delta\left(\frac{\tau}{\pi}\tan\frac{\phi}{2} + \frac{1}{\pi}\ln\left|\frac{\sin((\phi+\tau)/2)}{\sin((\phi-\tau)/2)}\right|\right) \tag{28a}$$

Table 3 Comparison of predicted lift and moment coefficients for an airfoil with 30% flap chord and 30° flap deflection

No. of elements	Present method 5 (3,2)[a]	Present method 8 (5,3)	VLM 5 (3,2)	VLM 8 (5,3)	Exact[6]
c_l	2.18371	2.17012	2.03596	2.08531	2.17377
c_m	−0.88522	−0.87914	−0.84667	−0.85962	−0.87936
C (Square-root singularity parameter)	0.38735	0.38543			0.38643
Hinge moment coeff. based on flap chord	−0.46151	−0.49813	−0.56554	−0.54415	−0.50548

[a] The second number is the number of elements on flap.

$$c_l = 2\delta(\tau + \sin\tau) \tag{28b}$$

$$c_m = -\delta(\tau/2 + \sin\tau + (\sin 2\tau)/4) \tag{28c}$$

where $\tau = \cos^{-1}(2x_f - 1)$ and $\phi = \cos^{-1}(2x - 1)$. In the VLM, equal spacing in each of the intervals has been used. For 8 vortex elements with $N_1 = 5$ and $N_2 = 3$, the results for the γ distribution for $\delta = 30°$ (or 0.5236 radian) and $x_f = 0.7$ are compared in Table 2. It is seen that the VLM produces relatively large error in the predicted γ distribution near all singularities. In making the comparison, it should be noted that the predicted γ values in both methods are at different locations. The primary error in the present method occurs near the logarithmic singularity. The lift and moment coefficients are compared in Table 3. The VLM tends to underestimate c_l and c_m. The same fact has also been recognized by Giesing (see Fig. 11 of Ref. 2). Geising[2] has noted that uneven spacing of the vortex elements can slightly improve the solution. However, the predicted lift coefficient is still too low. From the above comparison, it is evident that the present method gives more accurate results than the VLM does for a flapped airfoil.

III. Three-Dimensional Theory

A) Formulation

From the two-dimensional formulation, it is seen that the present method differs from the VLM only in the weighted sum for the chordwise integral and in the choice

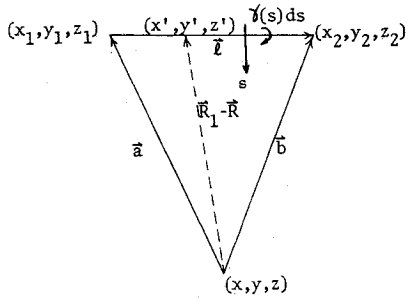

Fig. 1 Vortex segment geometry.

of vortex and control locations. Therefore, the present concept can be easily extended to any three-dimensional configuration, planar or nonplanar, without difficulty. This point will be further discussed later in Sec. IV. However, for algebraic simplicity, detailed derivation will be presented only for a planar wing without flap deflection.

To apply the above theory to a thin wing of finite aspect ratio, it is assumed that for the purpose of satisfying the wing tangency condition, the continuous vortex distribution over the wing is replaced with a quasi-continuous one, being continuous chordwise but step-wise constant in the spanwise direction. Thus, the wing surface is now covered with a number of vortex strips with the associated trailing vortices. In any strip, consider a vortex element γdx with an arbitrary direction $\mathbf{l}$ (see Fig. 1, where s is a coordinate with which the vortex strength will vary and has been replaced by x here). The integration of the induced velocities in the chordwise direction due to all vortex elements in the strip gives (see Appendix)

$$\mathbf{q}_1(\mathbf{R}) = \frac{\beta^2}{4\pi}\int_{x_l}^{x_t}\gamma(x')dx'\frac{\mathbf{a}\times\mathbf{l}}{|\mathbf{a}'\times\mathbf{l}'|^2}\left\{\frac{\mathbf{b}'}{|\mathbf{b}'|}-\frac{\mathbf{a}'}{|\mathbf{a}'|}\right\}\cdot\mathbf{l}' \tag{29}$$

due to the bounded vortex distribution and (See p. 43 of Ref. 8)

$$\mathbf{q}_2(\mathbf{R}) = \frac{\beta^2}{4\pi}\int_{x_l}^{x_t}\gamma(x')dx'\int_{x_i}^{\infty}\frac{(\mathbf{R}_1-\mathbf{R})\times d\mathbf{l}}{\mathbf{R}_\beta^3} \tag{30}$$

due to the associated trailing vortices.

For applications in thin wing theory, it can be shown that

$$\mathbf{a}'\times\mathbf{l}' = \beta\mathbf{k}\{(x_1-x)(y_2-y_1)-(x_2-x_1)(y_1-y)\}$$

$$\mathbf{b}'\cdot\mathbf{l}' = (x_2-x_1)(x_2-x)+\beta^2(y_2-y_1)(y_2-y)$$

$$\mathbf{a}'\cdot\mathbf{l}' = (x_2-x_1)(x_1-x)+\beta^2(y_2-y_1)(y_1-y)$$

It follows that Eq. (29) gives the following downwash integral:

$$w_1 = \mathbf{q}_1\cdot\mathbf{k} = \frac{1}{4\pi}\int_{x_l}^{x_t}\frac{\gamma(x')}{(x_1-x)(y_2-y_1)-(x_2-x_1)(y_1-y)}\cdot\left\{\frac{(x_2-x_1)(x_2-x)+\beta^2(y_2-y_1)(y_2-y)}{[(x_2-x)^2+\beta^2(y_2-y)^2]^{1/2}}-\frac{(x_2-x_1)(x_1-x)+\beta^2(y_2-y_1)(y_1-y)}{[(x_1-x)^2+\beta^2(y_1-y)^2]^{1/2}}\right\}dx' \tag{31}$$

Assuming straight trailing vortices on the wing plane, the integral in Eq. (30) can be reduced to

$$\int_{x_1}^{\infty}\frac{(\mathbf{R}_1-\mathbf{R})\times d\mathbf{l}}{R_\beta^3} = \int_{x_1}^{\infty}\frac{[(x_s-x)\mathbf{i}+(y_1-y)\mathbf{j}]\times(-\mathbf{i}dx_s)}{[(x_s-x)^2+\beta^2(y_1-y)^2]^{3/2}} = \frac{\mathbf{k}}{\beta^2(y_1-y)}\left[1-\frac{x_1-x}{((x_1-x)^2+\beta^2(y_1-y)^2)^{1/2}}\right] \tag{32}$$

Hence, the downwash due to the trailing vortex from the first end point (x_1, y_1) of the bounded vortex segment is

$$w_2'(x,y) = \frac{1}{4\pi}\int_{x_l}^{x_t}\frac{\gamma(x')}{y_1-y}\left[1-\frac{x_1-x}{((x_1-x)^2+\beta^2(y_1-y)^2)^{1/2}}\right]dx' \tag{33}$$

In the same manner, the downwash due to the trailing vortex from the second end point (x_2, y_2) of the bounded vortex segment is (noting that $d\mathbf{l} = \mathbf{i}dx_s$)

$$w_2''(x,y) = -\frac{1}{4\pi}\int_{x_l}^{x_t}\frac{\gamma(x')}{y_2-y}\left[1-\frac{x_2-x}{((x_2-x)^2+\beta^2(y_2-y)^2)^{1/2}}\right]dx' \tag{34}$$

Thus, the total downwash produced by a vortex strip is the sum of w_1, w_2', and w_2''.

For a rectangular horseshoe vortex element, $x_1 = x_2$ and Eq. (31) shows the usual Cauchy singularity in the x direction. For skewed elements, with y inside the element under consideration, and if y (the y-coordinate of a control point) is chosen so that $y_1 - y = K'(y_1 - y_2)$, where K' is some constant less than one, the expression in the denominator of Eq. (31) can be written as

$$\begin{aligned}&(x_1-x)(y_2-y_1)-(x_2-x_1)(y_1-y)\\&\quad=(y_2-y_1)[(x_1-x)+K'(x_2-x_1)]\\&=(y_2-y_1)[x_1+(x_2-x_1)(y-y_1)/(y_2-y_1)-x]\end{aligned} \tag{35}$$

which vanishes on the vortex segment at the chosen y-coordinate. Thus, the Cauchy singularity exists and the method of integration described in the two-dimensional theory is applicable.

For notational convenience, let

$$G_1(x',x,y) = \frac{(x_2-x_1)(x_2-x)+\beta^2(y_2-y_1)(y_2-y)}{[(x_2-x)^2+\beta^2(y_2-y)^2]^{1/2}} - \frac{(x_2-x_1)(x_1-x)+\beta^2(y_2-y_1)(y_1-y)}{[(x_1-x)^2+\beta^2(y_1-y)^2]^{1/2}} \tag{36}$$

$$G_2(x',x,y) = \frac{1}{y_1-y}\left[1-\frac{x_1-x}{((x_1-x)^2+\beta^2(y_1-y)^2)^{1/2}}\right] \tag{37}$$

$$G_3(x',x,y) = \frac{1}{y_2-y}\left[1-\frac{x_2-x}{((x_2-x)^2+\beta^2(y_2-y)^2)^{1/2}}\right] \tag{38}$$

The total downwash due to a strip of vortex distribution is therefore given by

$$w(x,y) = \frac{1}{4\pi}\int_{x_l}^{x_t}\frac{G_1(x',x,y)\gamma(x')dx'}{(x_1-x)(y_2-y_1)-(x_2-x_1)(y_1-y)} + \frac{1}{4\pi}\int_{x_l}^{x_t}G_2(x',x,y)\gamma(x')dx' - \frac{1}{4\pi}\int_{x_l}^{x_t}G_3(x',x,y)\gamma(x')dx' \quad (39)$$

The wing boundary condition is given by

$$w(x,y) = dz_c/dx - \alpha \quad (40)$$

Transforming the integration variable to a nondimensional one based on the local chord and then to the Θ-coordinate, Eq. (39) can be reduced to a finite sum as follows:

$$w(x,y) = \frac{1}{4\pi}\frac{\pi c}{N}\sum_{k=1}^{N}\frac{G_1(\theta_k)\gamma(\theta_k)(\sin\theta_k)/2}{(x_{1k}-x)(y_2-y_1)-(x_{2k}-x_{1k})(y_1-y)} + \frac{1}{4\pi}\frac{\pi c}{N}\sum_{k=1}^{N}G_2(\theta_k)\gamma(\theta_k)(\sin\theta_k)/2 - \frac{1}{4\pi}\frac{\pi c}{N}\sum_{k=1}^{N}G_3(\theta_k)\gamma(\theta_k)(\sin\theta_k)/2 \quad (41)$$

where

$$x_{1k} = x_{l_1} + c_1\xi_k, x_{2k} = x_{l_2} + c_2\xi_k,$$
$$\xi_k = [1-\cos((2k-1)\pi/2N)]/2, k = 1,2,\cdots,N \quad (42)$$

So far, the control-point locations have not been chosen yet. In accordance with the consideration in the two-dimensional theory, the x-coordinates of the control points should be chosen so that

$$x_i = x_l + c[1-\cos(i\pi/N)]/2, i = 0,1,2,\cdots,N \quad (43)$$

where x_l is the leading edge x-coordinate on the chord c through the control point. To choose the y control location, it should be noted that in the conventional VLM the spanwise vortex strips are usually of equal width and the y control locations are chosen to be at the midstrip. On the other hand, it is reasonable to assume that better results could be obtained if finer vortex strips are used in the region of rapid variation of sectional properties. For the latter, the well-known "semicircle" method is suitable for this purpose. In fact, this "semicircle" method has already been used in choosing the chordwise vortex points and control locations. Both equal and unequal spanwise vortex strips as mentioned above have been numerically experimented. Better results have been obtained with unequal spanwise vortex strips. Therefore, only the results by the latter method will be reported here. For a given planform, the semispan is divided into a suitable number of sections according to the wing-edge discontinuities. As illustrated in Fig. 2, the semispan has been divided into 2 sections. Each section is then divided into vortex strips by the semicircle method. Since the outermost stations in the semicircle method do not coincide with the endpoints, this procedure will create gaps between spanwise sections. These gaps must be eliminated, as illustrated in Fig. 2.

Any interval can be transformed into $[0,\pi]$ on the ϕ-plane. For example, any station y in the interval $[l_1, b/2]$ can be expressed in terms of ϕ through the relation:

$$y = (b/2 + l_1)/2 - (1/2)(b/2 - l_1)\cos\phi \quad (44)$$

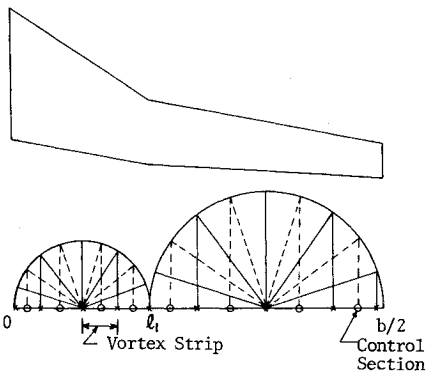

Fig. 2 Scheme of spanwise vortex strip distribution.

Thus $[l_1, b/2]$ is transformed into $[0,\pi]$. Let the vortex strips be chosen so that

$$(y_j - l_1)/(b/2 - l_1) = [1-\cos((2j-1)\pi/2M_2)]/2, j = 1,\cdots,M_2 \quad (45)$$

and the control points given by

$$(y_i - l_1)/(b/2 - l_1) = [1-\cos(i\pi/M_2)]/2, i = 1,\cdots,M_2 - 1 \quad (46)$$

Similar consideration is also applicable to the interval $[0,l_1]$ with M_2 replaced by M_1. Using the control points given by Eqs. (43) and (46) in Eqs. (41) and (40), the downwash influence coefficient can be immediately written down and Eq. (40) solved for the unknown γ.

To find the leading edge suction parameter, note that the leading edge suction term comes only from the bounded vortex distribution, and hence, from Eq. (31). Transforming Eq. (31) to the Θ-coordinate, and noting that Eq. (35) can be written as

$$(x_1-x)(y_2-y_1)-(x_2-x_1)(y_1-y) = (y_2-y_1)(\cos\theta-\cos\theta')c/2,$$

It is found that

$$w_1(x,y) = \frac{1}{4\pi}\int_0^{\pi}\frac{G_1(\theta')\gamma(\theta')\sin\theta'd\theta'}{(y_2-y_1)(\cos\theta-\cos\theta')} \simeq \frac{1}{4\pi}\frac{\pi}{N}\sum_{k=1}^{N}\left\{\frac{G_1(\theta_k)\gamma(\theta_k)\sin\theta_k - G_1(\theta)\gamma(\theta)\sin\theta}{(y_2-y_1)(\cos\theta-\cos\theta_k)}\right\} \quad (47)$$

in accordance with the concept discussed previously in relation to Eqs. (9) and (10). As shown before,

$$\sum_{k=1}^{N}\frac{1}{\cos\theta-\cos\theta_k} = N^2 \text{ if } \theta = 0, \qquad \lim_{\theta\to 0}\gamma(\theta)\sin\theta = 2C \quad (48)$$

Now,

$$\lim_{\theta\to 0}\frac{G_1(\theta)}{y_2-y_1} = \frac{1}{y_2-y_1}\left\{\frac{(x_{l_2}-x_{l_1})(x_{l_2}-x_l)+\beta^2(y_2-y_1)(y_2-y_l)}{[(x_{l_2}-x_l)^2+\beta^2(y_2-y_l)^2]^{1/2}} - \frac{(x_{l_2}-x_{l_1})(x_{l_1}-x_l)+\beta^2(y_2-y_1)(y_1-y_l)}{[(x_{l_1}-x_l)^2+\beta^2(y_1-y_l)^2]^{1/2}}\right\}$$

Since

$$(x_{l_2}-x_l)/(y_2-y_l) = (x_{l_2}-x_{l_1})/(y_2-y_1) = \tan\Lambda_l,$$
$$(x_l-x_{l_1})/(y_l-y_1) = (x_{l_2}-x_{l_1})/(y_2-y_1) = \tan\Lambda_l, \quad (49)$$

it follows that

$$\lim_{\theta\to 0}\frac{G_1(\theta)}{y_2 - y_1} = 2(\tan^2\Lambda_l + \beta^2)^{1/2} \tag{50}$$

Thus, the second term in Eq. (47) becomes

$$\lim_{\theta\to 0} -\frac{1}{4N}\sum_{k=1}^{N}\frac{G_1(\theta)\gamma(\theta)\sin\theta}{(y_2 - y_1)(\cos\theta - \cos\theta_k)} = -NC(\tan^2\Lambda_l + \beta^2)^{1/2} \tag{51}$$

If Eq. (51) is used in Eq. (41) which must be summed spanwise, it is found from Eq. (40) that at $x = x_l$,

$$\begin{aligned} NC(\tan^2\Lambda_l + \beta^2)^{1/2} &= \sum\frac{C}{4N}\sum_{k=1}^{N}\frac{G_1(\theta_k)\gamma(\theta_k)(\sin\theta_k)/2}{(x_{1k} - x)(y_2 - y_1) - (x_{2k} - x_{1k})(y_1 - y)} \\ &\quad + \sum\frac{C}{4N}\sum_{k=1}^{N}G_2(\theta_k)\gamma(\theta_k)(\sin\theta_k)/2 \\ &\quad - \sum\frac{C}{4N}\sum_{k=1}^{N}G_3(\theta_k)\gamma(\theta_k)(\sin\theta_k)/2 - \left(\frac{dz_c}{dx} - \alpha\right) \end{aligned} \tag{52}$$

where the unmarked summation is to be performed in the spanwise direction. Once the parameter C for each strip has been obtained, the magnitude of the sectional leading-edge thrust coefficient c_t can be computed:[9]

$$c_t = \frac{\pi}{8c}\frac{1}{\cos\Lambda_l}(1 - M_\infty^2\cos^2\Lambda_l)^{1/2}[\lim_{x\to x_l}\Delta C_p(x - x_l)^{1/2}]^2$$

where $\lim_{x\to x_l}\Delta C_p(x - x_l)^{1/2} = \lim_{x\to x_l} 2\gamma(x)(x - x_l)^{1/2} = 2C(c)^{1/2}$. Hence,

$$c_t = \pi C^2(1 - M_\infty^2\cos^2\Lambda_l)^{1/2}/(2\cos\Lambda_l) \tag{53}$$

For a skewed bounded element, the total vortex density of the element is $\gamma\Delta y/\cos\Psi$, where Δy is the strip width and Ψ is the element sweep angle. Its lift-producing component is obtained by multiplying by $\cos\Psi$. It follows that the lift-producing vortex density per unit span is γ. The sectional lift coefficient is therefore

$$c_l = \int_0^\pi \gamma(\theta)\sin\theta d\theta \cong \frac{\pi}{N}\sum_{k=1}^{N}\gamma_k\sin\theta_k \tag{54}$$

Similarly, the sectional pitching moment coefficient referred to the y-axis is

$$c_m = -\frac{2}{\bar{c}}\int_0^1 \gamma(\xi)(x_l + c\xi)d\xi \cong -\frac{\pi}{N\bar{c}}\sum_{k=1}^{N}\gamma_k\sin\theta_k(x_l + c\xi_k) \tag{55}$$

where ξ_k was given in Eq. (42). The sectional drag coefficient is

$$c_{di} = c_l\alpha - c_t \tag{56}$$

The total lift coefficient can be computed as follows:

$$\begin{aligned} C_L &= \frac{1}{S_w}\int_{-b/2}^{b/2}c_l c dy = \frac{2}{S_w}\left\{\int_0^{l_1}c_l c dy + \int_{l_1}^{b/2}c_l c dy\right\} \\ &= \frac{2}{S_w}\left\{\frac{l_1}{2}\int_0^\pi c_l c\sin\phi d\phi + \frac{b/2 - l_1}{2}\int_0^\pi c_l c\sin\phi d\phi\right\} \\ &\cong \frac{2}{S_w}\left\{\frac{l_1}{2}\frac{\pi}{M_1}\sum_{i=1}^{M_1 - 1}c_{li}c_i\sin\phi_i + \frac{b/2 - l_1}{2}\frac{\pi}{M_2}\sum_{i=1}^{M_2 - 1}c_{li}c_i\sin\phi_i\right\} \end{aligned} \tag{57}$$

where the integrals have been reduced to a finite sum by the conventional trapezoidal rule and ϕ_i are $i\pi/M_1$ or $i\pi/M_2$. Note that in the conventional trapezoidal rule, the values of the integrand at both integration limits appear in the finite sum. In the present case, both values are zero, because $\sin\phi = 0$ at $\phi = 0$ and π. The values of ϕ_i coincide with the y-control location given in Eq. (46). The total pitching moment coefficient C_m and the total thrust coefficient C_T can be found in a similar manner. The total induced drag coefficient is given by

$$C_{Dii} = C_L\alpha - C_T \tag{58}$$

In the thin wing theory, the convergence of solutions is indicated by the agreement of the near-field and the far-field induced drags. The far-field induced drag is given by [Eq. (143) of Ref. 10]:

$$C_{Di} = \frac{1}{S_w}\int_{-b/2}^{b/2}c_l c\alpha_i dy \tag{59}$$

where α_i is the induced angle of attack given by [Eq. 61 of Ref. (10)]

$$\alpha_i = -\frac{1}{8\pi}\int_{-b/2}^{b/2}\frac{c_l c}{(y - y')^2}dy' \tag{60}$$

Using Multhopp's interpolation formula for $c_l c$:

$$c_l c = \frac{2}{M}\sum_{n=1}^{M-1}(c_l c)_n\sum_{\lambda=1}^{M-1}\sin\lambda\phi_n\sin\lambda\phi \tag{61}$$

where

$$\phi_n = n\pi/M,\ n = 1, \cdots, M - 1, \tag{62}$$

Eq. (60) can be integrated, with $y = -(b/2)\cos\phi$, resulting in

$$\alpha_i = (1/8b)\sum_{n=1}^{M-1}(c_l c)_n b_{n\nu} \tag{63}$$

where

$$b_{n\nu} = \frac{(-1)^{n-\nu} - 1}{M}\frac{2\sin\phi_n}{(\cos\phi_n - \cos\phi_\nu)^2},\ n \neq \nu \tag{64a}$$

$$= M/\sin\phi_\nu,\ n = \nu \tag{64b}$$

$$\phi_\nu = \nu\pi/M,\ \nu = 1, \cdots, M - 1 \tag{65}$$

Once α_i's are obtained from Eq. (63), Eq. (59) can be integrated to give

$$C_{Di} = \frac{b}{2S_w}\frac{\pi}{M}\sum_{i=1}^{M-1}(c_l c\alpha_i)_i\sin\phi_i \tag{66}$$

where ϕ_i is given by Eq. (65) with ν replaced by i.

In Eq. (63), c_l's and c's at stations specified by Eq. (62) are required. However, only those at stations given by Eq. (46) are known. Therefore, some interpolation procedure must be used. In the present method, the Lagrange interpolation formula was used for obtaining any intermediate values.

B) Comparison with Known Results

In the following illustration of the present method, M is taken to be 31, except for the variable-sweep wing where $M = 41$. It is assumed that the convergence of solutions is achieved if the near-field induced drag differs from the far-field value by less than 1%. The results for four planforms are tabulated in Tables 4–7. The methods chosen for comparison include the VLM and some continuous loading methods [NLR's[11] (The National Aerospace Laboratory of the Netherlands), Lamar's[12] and Wagner's[13]]. The geometry of the rectangular and delta wings is self-evident. The geometrical details of Warren 12 and variable-sweep wings are given in Figs. 3 and 4. The conver-

Table 4 Aerodynamic characteristics of a rectangular wing of $A = 2$ at $M_\infty = 0$

Method	$C_{L\alpha}$,rad^{-1}	$C_{m\alpha}$,rad^{-1}	C_{Dii}/C_L^2	C_{Dii}/C_{Di} (C_T/C_T')
Present $N_c = 8, N_s = 15$	2.4707	−0.5173	0.1595	0.9972
VLM[1] $N_c = 6, N_s = 20$	2.5239	−0.5334	0.1554	0.9747
NLR[11]	2.4744	−0.5182	0.1609	1.0101
Wagner[13]	2.4778	−0.5180	0.1619	1.0167 (0.9891)

Table 5 Aerodynamic characteristics of a delta wing of A = 2 at $M_\infty = 0.13$ and $\alpha = 4.3°$

Method	C_L	a.c.[a]	C_{Dii}/C_L^2	C_{Dii}/C_{Di} (C_T/C_T')
Present $N_c = 3, N_s = 35$	0.1649	0.3767	0.1625	1.0078
Lamar[12]	0.168	0.363		
VLM[1] $N_c = 6, N_s = 20$ $(M_\infty = 0.1)$	0.1654	0.3823	0.1549	0.9655
Wagner[13]	0.1663	0.3783	0.1576	0.9795 (1.01137)
Experiment[12]	0.159	0.396		

[a] Measured from the leading edge of the mean aerodynamic chord.[12]

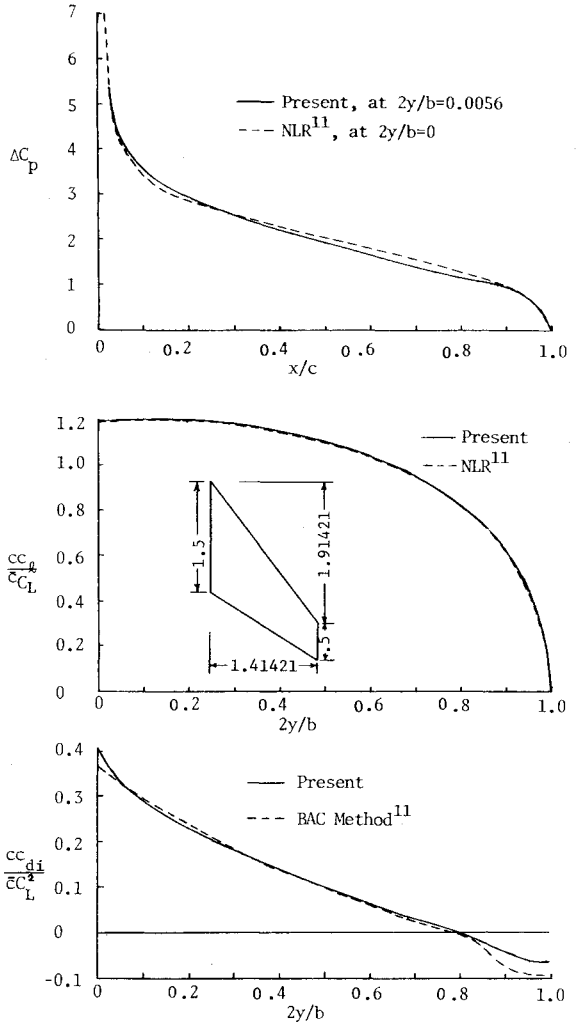

Fig. 3 Comparison of predicted aerodynamic characteristics for Warren 12 planform at $M_\infty = 0$.

Table 6 Aerodynamic characteristics of Warren 12 planform of $A = 2(2)^{1/2}$ at $M_\infty = 0$

Method	$C_{L\alpha}$,rad^{-1}	$C_{m\alpha}$,rad^{-1}	C_{Dii}/C_L^2	C_{Dii}/C_{Di}
Present $N_c = 5, N_s = 20$	2.7382	−3.0844	0.11428	1.0054
VLM[1] $N_c = 5, N_s = 15$	2.7944	−3.1775	0.1055	0.9275
NLR[11] $(m = 15)$	2.7373	−3.1074	0.1201	1.0564
NLR[11] $(m = 31)$	2.7576	−3.1155	0.1135	0.9921

Table 7 Aerodynamic characteristics of a variable-sweep wing of $A = 4.303$ at $M_\infty = 0.23$

Method	$C_{L\alpha}$,rad^{-1}	a.c.[a]	C_{Dii}/C_L^2	C_{Dii}/C_{Di}
Present $N_c = 4, N_s = 28$	3.0070	−0.1378	0.0760	0.9989
VLM[14] $N_c = 5, N_s = 32$	3.02485		0.07465	0.9815
Wagner[13]	2.844		0.075	1.0
Lamar[12]	3.057	−0.175		
Experiment[12]	2.75	−0.106		

[a] Measured from the leading edge of the mean aerodynamic chord.[12]

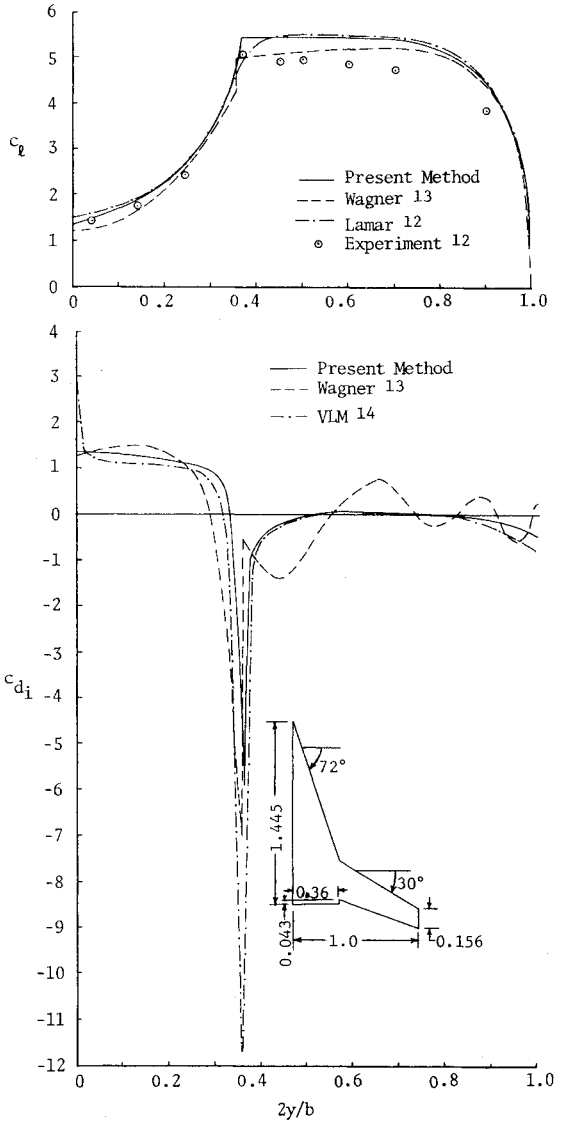

Fig. 4 Comparison of predicted aerodynamic characteristics for a variable-sweep wing of $A = 4.303$ at $M_\infty = 0.23$ and $\alpha = 1$ radian.

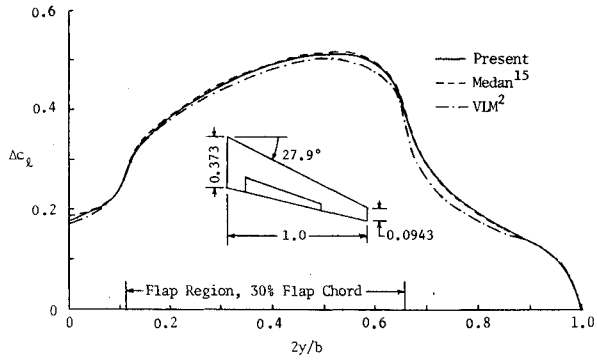

Fig. 5 Comparison of predicted lift increments for a wing with partial span flap deflection at $M_\infty = 0.2$ and $\alpha = 10°$. Flap angle = 10°.

gence of solutions in Wagner's program[13] is indicated by the agreement of the near-field thrust coefficient C_T and the far-field C_T'. Their ratios are given in the parentheses under C_{Dii}/C_{Di} in Tables 4 and 5. It is seen that the conventional VLM tends to yield higher $C_{L\alpha}$ and $-C_{m\alpha}$ and lower $C_{Dii}/C_L{}^2$. Hough[5] has shown for the rectangular wing of $A = 2$ and the Warren 12 planform that $C_{L\alpha}$ and $C_{Dii}/C_L{}^2$ can be improved by wing tip inset. From the comparison, it is seen that the present method always gives good results for the total aerodynamic characteristics.

The predicted pressure distribution at the plane of symmetry and the span loading for the Warren 12 planform are compared with the results of NLR[11] in Fig. 3. The agreement is good. Since Ref. 11 does not include the induced drag distribution by the NLR method, the results by the BAC (British Aircraft Corporation) method are compared instead. Again, the agreement is good. The distribution of the sectional lift and induced drag coefficients for the variable-sweep wing is given in Fig. 4. The c_l distribution is seen to agree quite well with Lamar's method,[12] while the c_{di} distribution is very close to that given by the VLM.[14] It should be noted that the VLM results have been scaled by a factor equal to C_{Di}/C_{Dii} and have been computed with 160 vortices, compared with 112 vortices in the present method.

To illustrate the accuracy and efficiency of the present method for a wing with flap deflection, a planform of $A = 8.56$ with partial span flap deflection is selected. The difference in the section lift coefficient for the wing with and without the flap deflected at $\alpha = 10°$ is presented in Fig. 5, together with the VLM results[2] and Medan's.[15] Medan's method is an extension of Wagner's[13] by including the flap pressure mode in the formulation. The agreement with the continuous loading method of Medan's is seen to be quite good. The present results are computed with 5 chordwise vortices and 20 spanwise strips. When the number of chordwise vortices are increased to 8, the results are changed by only 0.2%. It is of interest to note that Giesing[2] has suggested 14 chordwise vortex elements for wings with flaps in the VLM method for an error not greater than 5%. Therefore, the present method is seen to be efficient and accurate even for a wing with partial span flap deflection.

As far as the computer processing time is concerned, the present method is as economical as the VLM. With 100 unknown vortex strengths, the present program requires 1 min of processing time by the Honeywell 635 computer. On the other hand, the Wagner's program, when run on the same computer, requires more computing time for a converged solution, from 3 times more for unswept wings to 7 times more for low aspect-ratio highly swept wings.

IV. Discussions of Nonplanar Applications

Even though only plane wing results have been presented, the present method is by no means restricted to planar configurations. For applications to any nonplanar configurations, it is necessary to retain all three Cartesian components for all vector quantities in Eqs. (29) and (30). No matter whether the control points are on the vortex surface or not, the vortex integrals can always be approximated by finite sums through midpoint trapezoidal rule after the Θ-transformation is made to remove the square-root singularities and weaken the logarithmic singularity if any. The Cauchy singularity if any is automatically accounted for because of the particular choice of the control and integration points. Therefore, if the present sets of vortex and control locations as prescribed in Eqs. (42) and (43) are used, the VLM formulation for solving the unknown vortex distribution can be easily modified as follows. Division by 4π in the influence matrix elements of the VLM is replaced by multiplication of an appropriate factor $c \sin \Theta/(8N)$ for each aerodynamic section in accordance with Eq. (41). A user may divide any complicated configuration into several aerodynamic sections as he sees fit, such as main wing section, flap section, tail, body, etc., exactly in the same manner as in the VLM formulation. The resulting matrix equation for the vortex distribution is then solved in the usual way. Of course, the leading edge thrust distribution is computed in a different manner. In the present method, the total induced downwash at the leading edge is summed first in order to compute the parameter C according to Eq. (52) and Eq. (53) is then used to find the thrust coefficient. The computation of force and moment coefficients, being done by the trapezoidal rule, would present no difficulty. As the near-field solution for the induced drag has been proved to be accurate, the far-field computation as given in Eqs. (59)–(66) can be disregarded in any nonplanar applications.

This method has already been successfully applied to a lifting surface theory for the wing slipstream interaction problem with the angle-of-attack effect, flap deflections, and Mach number nonuniformity. The results will be reported later. From the author's experience with both the VLM and the present method, the present method not only is as simple as the VLM to apply, but also has the same generality. However, the present method has the following advantages: good accuracy for a given number of vortex elements employed, good efficiency so that not too many vortex elements are needed for a given accuracy and its simple theoretical foundation in derivation.

V. Conclusions

A quasi-continuous method in thin wing theory has been developed in detail. Unlike the conventional vortex lattice method, the wing-edge square-root singularities and the Cauchy singularity have been properly accounted for in this method. It has been shown that all aerodynamic characteristics in thin airfoil theory, including the leading edge suction and the pressure distribution, are exactly reproduced for a flat airfoil. For an airfoil with flap deflection, the present approximation is more accurate than the VLM. The planar lifting-surface results are comparable to those by some continuous loading methods. However, the present method requires much less computing time in some comparison. The objection to the leading-edge thrust distribution over the chord in the VLM has been removed by employing a different approach to the problem. The method can be easily extended to nonplanar configurations, so that the simplicity and the generality of the VLM have been retained.

Appendix

The velocity field due to a line segment of vortex of strength Γ in the linearized compressible flow is given by[8]

$$\mathbf{v}(\mathbf{R}) = \frac{\beta^2\Gamma}{4\pi}\int_l \frac{(\mathbf{R}_1 - \mathbf{R}) \times \mathbf{dl}}{R_\beta{}^3} \tag{A1}$$

Define a parameter τ such that

$$\mathbf{R}_1 - \mathbf{R} = \mathbf{a} + \tau\mathbf{l} \tag{A2}$$

Expressing R_β in terms of τ, it can be shown that Eq. (A1) can be reduced to

$$\mathbf{v}(\mathbf{R}) = \frac{\beta^2\Gamma}{4\pi}\mathbf{a}\times\mathbf{l}\int_0^1 \frac{d\tau}{[\bar{A}\tau^2 + \bar{B}\tau + \bar{C}]^{3/2}}$$

$$= \frac{\beta^2\Gamma}{4\pi}\mathbf{a}\times\mathbf{l}\left\{\frac{2\bar{B}}{(\bar{B}^2 - 4\bar{A}\bar{C})\bar{C}^{1/2}} - \frac{2(2\bar{A} + \bar{B})}{(\bar{B}^2 - 4\bar{A}\bar{C})(\bar{A} + \bar{B} + \bar{C})^{1/2}}\right\}, \quad \bar{B}^2 - 4\bar{A}\bar{C} \neq 0 \tag{A3}$$

where $\bar{A} = |\mathbf{l}'|^2$, $\bar{B} = 2\mathbf{a}'\cdot\mathbf{l}'$ and $\bar{C} = |\mathbf{a}'|^2$. Further, it can be shown that

$$\bar{B}^2 - 4\bar{A}\bar{C} = -4\,|\mathbf{a}'\times\mathbf{l}'|^2 \tag{A4}$$

$$2\bar{A} + \bar{B} = 2\mathbf{b}'\cdot\mathbf{l}' \tag{A5}$$

$$\bar{A} + \bar{B} + \bar{C} = |\mathbf{b}'|^2 \tag{A6}$$

It follows that Eq. (A5) becomes

$$\mathbf{v}(\mathbf{R}) = \frac{\beta^2\Gamma}{4\pi}\frac{\mathbf{a}\times\mathbf{l}}{|\mathbf{a}'\times\mathbf{l}'|^2}\left\{\frac{\mathbf{b}'}{|\mathbf{b}'|} - \frac{\mathbf{a}'}{|\mathbf{a}'|}\right\}\cdot\mathbf{l}' \tag{A7}$$

Another form for Eq. (A7) can be obtained by eliminating $\mathbf{l}$ and $\mathbf{l}'$ to give

$$\mathbf{v}(\mathbf{R}) = \frac{\beta^2\Gamma}{4\pi}\frac{\mathbf{a}\times\mathbf{b}}{|\mathbf{a}'\times\mathbf{b}'|^2}[|\mathbf{a}'| + |\mathbf{b}'|]\left[1 - \frac{\mathbf{a}'\cdot\mathbf{b}'}{|\mathbf{a}'|\,|\mathbf{b}'|}\right] \tag{A8}$$

For $\beta = 1$, Eq. (A8) reduces to the expression used by Maskew.[16]

References

[1]Margason, R. J. and Lamar, J. E., "Vortex-Lattice Fortran Program for Estimating Subsonic Aerodynamic Characteristics of Complex Planforms," TN D-6142, Feb. 1971, NASA.

[2]Giesing, J. P., "Lifting Surface Theory for Wing-Fuselage Combinations," Rept. DAC-67212, Vol. 1, Aug. 1968, Douglas Aircraft Co., Long Beach, Calif.

[3]Hancock, G. J., "Comment on 'Spanwise Distribution of Induced Drag in Subsonic Flow by the Vortex Lattice Methods'," *Journal of Aircraft*, Vol. 8, No. 8, Aug. 1971, p. 681.

[4]James, R. M., "On the Remarkable Accuracy of the Vortex Lattice Discretization in Thin Wing Theory," Rept. DAC-67211, Feb. 1969, Douglas Aircraft Co., Long Beach, Calif.

[5]Hough, G. R., "Remarks on Vortex-Lattice Methods," *Journal of Aircraft*, Vol. 10, No. 5, May, 1973, pp. 314–317.

[6]Spence, D. A., "The Lift on a Thin Aerofoil with a Jet-Augmented Flap," *Aeronautical Quarterly*, Vol. 9, Aug. 1958, pp. 287–299.

[7]Luke, Y. L., "The Special Functions and Their Approximations," Vol. II, Chap. XV, Academic Press, New York, 1969.

[8]Ward, G. N., "Linearized Theory of Steady High Speed Flow," Cambridge University Press, New York, 1955.

[9]Lan, C. and Roskam, J., "Leading-Edge Force Features of the Aerodynamic Finite Element Method," *Journal of Aircraft*, Vol. 9, No. 12, Dec. 1972, pp. 864–867.

[10]Multhopp, H., "Methods for Calculating the Lift Distribution of Wings (Subsonic Lifting-Surface Theory)," Reports and Memoranda 2884, Jan. 1950, Aeronautical Research Council, London, England.

[11]Garner, H. C., Hewitt, B. L., and Labrujere, T. E., "Comparison of Three Methods for the Evaluation of Subsonic Lifting-Surface Theory," Reports and Memoranda 3597, June 1968, Aeronautical Research Council, London, England.

[12]Lamar, J. E., "A Modified Multhopp Approach for Predicting Lifting Pressures and Camber Shape for Composite Planforms in Subsonic Flow," TN D-4427, July 1968, NASA.

[13]Wagner, S., "On the Singularity Method of Subsonic Lifting-Surface Theory," *Journal of Aircraft*, Vol. 6, No. 6, Nov.–Dec. 1969, pp. 549–558.

[14]Kálmán, T. P., Giesing, J. P. and Rodden, W. P., "Spanwise Distribution of Induced Drag in Subsonic Flow by the Vortex Lattice Method," *Journal of Aircraft*, Vol. 7, No. 6, Nov.–Dec. 1970, pp. 574–576.

[15]Medan, R. T., "Steady, Subsonic, Lifting Surface Theory for Wings with Swept, Partial Span, Trailing Edge Control Surfaces," TN D-7251, April 1973, NASA.

[16]Maskew, B., "Calculation of the Three-Dimensional Potential Flow Around Lifting Non-Planar Wings and Wing-Bodies Using a Surface Distribution of Quadrilateral Vortex-Rings," Rept. TT 7009, September, 1970, Dept. of Transport Technology, University of Technology, Loughborough, U.K.